The Astrophysical Journal, 786:110 (9pp), 2014 May 10 doi:10.1088/0004-637X/786/2/110

A POSSIBLE COLD IMPRINT OF VOIDS ON THE MICROWAVE BACKGROUND RADIATION

Yan-Chuan Cai[1], Mark C. Neyrinck[2], István Szapudi[3], Shaun Cole[1], and Carlos S. Frenk[1]
[1] Institute for Computational Cosmology, Department of Physics, University of Durham, South Road, Durham DH1 3LE, UK; y.c.cai@durham.ac.uk
[2] Department of Physics and Astronomy, The Johns Hopkins University, 3701 San Martin Drive, Baltimore, MD 21218, USA
[3] Institute for Astronomy, University of Hawaii, 2680 Woodlawn Drive, Honolulu, HI 96822, USA
Received 2013 October 25; accepted 2014 February 8; published 2014 April 24

ABSTRACT

We measure the average temperature decrement on the cosmic microwave background (CMB) produced by voids selected in the Sloan Digital Sky Survey Data Release 7 spectroscopic redshift galaxy catalog, spanning redshifts $0 < z < 0.44$. We find an imprint amplitude between 2.6 and 2.9 μK as viewed through a compensated top-hat filter scaled to the radius of each void, we assess the statistical significance of the imprint at $\sim 2\sigma$, and we make crucial use of *N*-body simulations to calibrate our analysis. As expected, we find that large voids produce cold spots on the CMB through the integrated Sachs–Wolfe (ISW) effect. However, we also find that small voids in the halo density field produce hot spots, because they reside in contracting, larger-scale overdense regions. This is an important effect to consider when stacking CMB imprints from voids of different radii. We have found that the same filter radius that gives the largest ISW signal in simulations also yields close to the largest detected signal in the observations. However, although it is low in significance, our measured signal has a much higher amplitude than expected from ISW in the concordance ΛCDM universe. The discrepancy is also at the $\sim 2\sigma$ level. We have demonstrated that our result is robust against the varying of thresholds over a wide range.

Key words: cosmic background radiation – cosmology: observations – large-scale structure of universe – methods: statistical

Online-only material: color figures

1. INTRODUCTION

The late-time integrated Sachs–Wolfe effect (ISW; Sachs & Wolfe 1967) is direct evidence of cosmic acceleration (Crittenden & Turok 1996). However, detection of the ISW effect by the cross-correlation of large-scale structure and the cosmic microwave background (CMB) is challenging because of large cosmic variance and possible systematics. A combined analysis of a few different galaxy/QSO surveys has yielded a signal of estimated significance 4σ (Giannantonio et al. 2008, 2012; Ho et al. 2008), although there are alternative views (e.g., Rassat et al. 2007; Sawangwit et al. 2010; Bielby et al. 2010; López-Corredoira et al. 2010; Hernández-Monteagudo 2010). These, and most other, analyses have used a cross-correlation function method.

Another method exploits the physical insight that in the presence of dark energy, linear-scale voids, and superclusters stretch faster than they can grow through gravity and thus produce cold and hot spots, respectively, in the CMB. Granett et al. (2008, hereafter G08) stacked 100 such quasilinear-scale structures, reporting a detection of corresponding cold and hot spots at 4σ significance. Even without dark energy, the potential can change on nonlinear scales, producing CMB imprints; this is known as the Rees–Sciama (RS) effect (Rees & Sciama 1968). We refer to the full effect as ISWRS. The nonlinear RS effect may confuse an interpretation of an ISW-like detection with a signal of dark energy, but it is expected only at the $\sim 10\%$ level at $z < 1$ on sub-degree scales (Cai et al. 2009; Smith et al. 2009; Cai et al. 2010). The significance level of the G08 detection from a single galaxy sample seems to be higher than that from the cross-correlation method, and the amplitude of the signal is found to be 2σ to 3σ higher than estimates from simulations; this indicates tension with the concordance cosmology at $z \sim 0.5$ (G08; Nadathur et al. 2012; Pápai & Szapudi 2010; Pápai et al. 2011). Incorporating the contribution of nonlinearity seems unable to reduce this tension (Nadathur et al. 2012; Flender et al. 2013; Hernandez-Monteagudo & Smith 2013). It is therefore important to check if such a signal/tension persists at other epochs of the universe and in other void catalogs.

In this paper, we reinvestigate this issue by using a new, independent Sloan Digital Sky Survey (SDSS) void catalog, which uses the ZOBOV (Neyrinck 2008) void-finder that G08 used.[4] Compared with G08, which used photometric redshifts, the current sample uses galaxies both with accurate spectroscopic redshifts and, at low redshift, much higher sampling, allowing more accurate knowledge of each void's physical structure. The current sample covers the redshift range $0 < z < 0.44$, complementing the previous catalog, which spans $0.4 < z < 0.75$.

Voids identified in a galaxy density field do not necessarily pick out the optimal structures for ISW detection. First, discrete sampling of the density field will lead to spurious voids from Poisson noise. Second, voids of the same density contrast and size may reside in different large-scale environments, changing their ISW signals. Pruning void catalogs is important for optimizing the ISW detection, but it is crucial to do so a priori (e.g., theoretically) rather than a posteriori, (e.g., claiming the largest detection over some ad hoc parameter). Indeed, using simulations, we are able to clean the void catalogs on the basis of physically motivated reasons *prior* to inspecting the results. This is an important step to avoid a posteriori bias in this type of analysis.

We appreciate that similar void catalogs constructed by Sutter et al. (2012) have been used independently for ISW detection (Ilić et al. 2013; Planck Collaboration et al. 2013b). Thus, we do not intend to repeat the same analysis using exactly the same

[4] The void catalog used in this paper can be obtained at http://skysrv.pha.jhu.edu/~mneyrinck/DR7voids.tar.gz

catalogs. Rather, we will use our own version of void catalogs, which have subtle differences than that of Sutter et al. (2012). Very recently, Nadathur & Hotchkiss (2013) produced another void catalog from the same volume-limited galaxy samples. While all these catalogs may differ from each other, it is unclear which is optimal for ISW detection. We discuss our results in the context of these recent measurements in the conclusion. In the present paper, we concentrated on aligning the void detection algorithm as close as possible between our simulations and the observations.

In Section 2 of our paper, we briefly describe the void catalog and details of the stacking procedure. Section 3 presents simulations of the void catalog and the ISWRS signal. The main results are presented in Section 4, including systematic tests. Conclusions and discussion are presented in Section 5.

2. VOID CATALOG

For our analysis, we use a set of voids detected from the SDSS Data Release 7 (DR7) main-galaxy sample (MGS; Strauss et al. 2002), and luminous-red-galaxy (LRG) sample (Eisenstein et al. 2001), covering 8500 deg^2 on the sky. These are the same galaxy catalogs as used for void finding by Sutter et al. (2012, hereafter S12). The MGS has a redshift range of $0 < z < 0.2$ and the LRG sample a range of $0.16 < z < 0.44$. Six volume-limited samples are made out of these two samples. They are *dim*1 ($0 < z < 0.05$), *dim*2 ($0.05 < z < 0.1$), *bright*1 ($0.1 < z < 0.15$), *bright*2 ($0.15 < z < 0.2$), *lrgdim* ($0.16 < z < 0.36$), and *lrgbright* ($0.36 < z < 0.44$). The number densities decrease with increasing sample redshift.

We use the original ZOBOV (Neyrinck et al. 2005; Neyrinck 2008) algorithm to find voids, both in the simulations and the observed samples. In the ZOBOV paper (Neyrinck 2008), ZOBOV is called "parameter-free"—indeed, it can return a parameter-free set of voids and subvoids, nested catchment basins around local density minima as detected in a watershed transform (e.g., Platen et al. 2007). A parameter-free Voronoi tessellation (e.g., Schaap & van de Weygaert 2000) is used to measure each galaxy's density and set of neighbors.

In ZOBOV's parameter-free mode, voids can far exceed what might be considered their most physically meaningful extent, since the largest void detected will encompass the entire survey, the density catchment around the global minimum-density galaxy. Therefore, we use a criterion to halt the joining of "zones" together to form voids. A "zone" is a subvoid, i.e., a density catchment, at the bottom of which is a local density minimum. Dividing zones from each other are density ridges, where density gradients head down to different density minima on either side. A zone z is not added to a void v if the lowest-density galaxy on the density ridge between v and z exceeds 0.2. This threshold value is the fiducial density of a top-hat void after shells cross on its edge, in the spherical expansion model (e.g., Sheth & van de Weygaert 2004). This step does not affect the number of voids (which corresponds exactly to the number of local density minima), but it does affect total void volumes that are used in our measurement.

There end up being some slight differences between our catalog and the Sutter et al. (2012) catalogs. We do not track down every difference, but we list here several slight differences in the implementation. Sutter et al. (2012) explicitly use hierarchical information in splitting voids from each other, which may result in slight differences in how voids are split at the edges (Sutter et al. 2013). They also eliminate voids with overdensities $\delta > -0.8$, as estimated in a top-hat sphere of radius $(1/4)r_v$ about the volume-weighted void center, where r_v is the effective void radius, $[3/(4\pi)V]^{1/3}$. Also, we explicitly remove voids with $\rho_{\rm min} \geqslant 1$ (where $\rho_{\rm min}$ is the minimum density of a void, and a density minimum is a galaxy with lower density than any of its neighbors), since for our particular application we do not want to use local density minima within obviously overdense regions.

To deal with the boundaries, we use the same set of buffer galaxies surrounding the survey as used by Sutter et al. (2012) (in their 2012 November catalog). Nadathur & Hotchkiss (2013) have found that this set of buffer galaxies is sparser than would be ideal and also that the positions of some bright stars were not considered in the analysis. These could result in some galaxy densities being corrupted. However, if these corrupted densities result in spurious voids, they should typically be eliminated by our strict cuts in the void's effective radius and minimum-to-ridge density contrast, as we describe below. Nadathur & Hotchkiss (2013) have also raised the concern that void detections can be unexpectedly sensitive to changes in the distance coordinate. Ideally, perhaps we would have used a ΛCDM distance estimate instead of the redshift distance cz. However, again we do not expect the choice of distance coordinate to matter substantially for the large voids that survive our conservative cuts. Also, importantly, any corruptions should only contribute to the noise, rather than to the signal, in our measurement.

3. SIMULATIONS

For testing our analysis pipeline and to understand the expected ISWRS signal, we construct mock ΛCDM void catalogs from N-body simulations and compute their expected ISWRS signal. Our goal is to perform the same analysis in the SDSS data as in our simulated voids, where the ISWRS signal is known.

3.1. Simulations of Voids

We construct mock void catalogs by using a set of simulations run in the concordance cosmology ($\Omega_{\rm m} = 0.24, \Omega_\Lambda = 0.76, n_s = 0.958, \sigma_8 = 0.77, h = 0.73$) (Li et al. 2013). The simulations are run with the following box sizes and numbers of particles: [$L = 1500$ Mpc h^{-1}, $N_{\rm p} = 1024^3$), [$L = 1000$ Mpc h^{-1}, $N_{\rm p} = 1024^3$), and [$L = 250$ Mpc h^{-1}, $N_{\rm p} = 512^3$]. We use halos matched to the number densities of galaxies in the 6 volume-limited subsamples of the SDSS data. We use halos with more than 20 particles, as linked by the Friends-of-Friends algorithm with the linking length of 0.2 (Davis et al. 1985). The particle masses in our simulations are $2.09 \times 10^{11}\ M_\odot\ h^{-1}$, $6.20 \times 10^{10}\ M_\odot\ h^{-1}$, and $0.77 \times 10^{10}\ M_\odot\ h^{-1}$, giving minimum halo masses $M_{\rm min} = 4.18 \times 10^{12}\ M_\odot\ h^{-1}$, $1.24 \times 10^{12}\ M_\odot\ h^{-1}$, and $1.54 \times 10^{11}\ M_\odot\ h^{-1}$. Halos are approximated as galaxies, assuming that each main halo hosts one SDSS galaxy. This simple treatment neglects the complexity of galaxy formation and halo occupation. In the densest galaxy samples, for example, large halos should host multiple galaxies, better delineating void edges. Excluding these extra galaxies may reduce our ability to detect voids in the simulations. However, given that we rely on halos just to find voids and that the typical sizes of voids are usually orders of magnitude larger than the size of halos, the simulated void catalog should be acceptable for our purposes.

To model the signal, it is important to match the galaxy sampling density, since more, and smaller, structures are found with increasing sampling. We adjust $M_{\rm min}$ to match the number density of galaxies except in the two lowest-redshift subsamples,

where the number density of galaxies are beyond the resolution limit of our current simulations. In principle, we could use a higher-resolution simulation to match these densities. But given that the volume of these two subsamples is less than 2% of the total, we expect them to contribute very little to the final stacked signal, which will be demonstrated in the next section. We therefore do not make the effort to analyze higher resolution simulations, and we leave it for future work. The two highest-redshift LRG subsamples have the largest average voids and dominate the volume. To reduce cosmic variance in the average signals, we employ six realizations of the simulation with $L = 1500$ Mpc h^{-1}.

We apply the same void finding algorithm as in the real data to these mock halo catalogs and find voids at four discrete redshift slices, a =0.7, 0.8, 0.9, 1.0 in the cubic simulation boxes, where $a = 1/(1+z)$ is the expansion factor. This covers the whole redshift range of the SDSS void catalog.

3.2. Simulations of ISW

For each simulation box, we follow the algorithm presented by Cai et al. (2010) (see also Seljak 1996; Smith et al. 2009; Nadathur et al. 2012; Hernandez-Monteagudo & Smith 2013) to compute the time derivative of the potential $\dot{\Phi}$ using particle data. This can be achieved by computing $\dot{\Phi}$ in Fourier space using

$$\dot{\Phi}(\boldsymbol{k},t) = \frac{3}{2}\left(\frac{H_0}{k}\right)^2 \Omega_{\rm m}\left[\frac{\dot{a}}{a^2}\delta(\boldsymbol{k},t) + \frac{i\boldsymbol{k}\cdot\boldsymbol{p}(\boldsymbol{k},t)}{a}\right], \quad (1)$$

where $\boldsymbol{p}(\boldsymbol{k},t)$ is the Fourier transform of the momentum density divided by the mean mass density, $\boldsymbol{p}(\boldsymbol{x},t) = [1+\delta(\boldsymbol{x},t)]\boldsymbol{v}(\boldsymbol{x},t)$, $\delta(\boldsymbol{k},t)$ is the Fourier transform of the density contrast, and H_0 and $\Omega_{\rm m}$ are the present values of the Hubble and matter density parameters. The inverse Fourier transform of the above yields $\dot{\Phi}$ in real space on three-dimensional (3D) grids. The integration of $\dot{\Phi}$ along the line of sight yields the full ISWRS temperature fluctuation,

$$\frac{\Delta T(\hat{n})}{T} = \frac{2}{c^2}\int \dot{\Phi}(\hat{n},t)dt. \quad (2)$$

In the linear regime, the velocity field is related to the density field by the linearized continuity equation $\boldsymbol{p}(\boldsymbol{k},t) = i\dot{\delta}(k,t)\boldsymbol{k}/k^2 \approx i\beta(t)\dot{a}/a\delta(k,t)\boldsymbol{k}/k^2$. Thus,

$$\dot{\Phi}(\boldsymbol{k},t) = \frac{3}{2}\left(\frac{H_0}{k}\right)^2 \Omega_{\rm m}\frac{\dot{a}}{a^2}\delta(\boldsymbol{k},t)[1-\beta(t)], \quad (3)$$

where $\beta(t)$ denotes the linear growth rate $\beta(t) \equiv d\ln D(t)/d\ln a$. This equation models the linear ISW effect, using only information from the density field. This approach has also been adopted by Watson et al. (2014) for larger volume simulations.

4. STACKING OF VOIDS

4.1. Stacking in Simulations

With the simulated void catalogs and the simulated ISWRS and ISW maps, we can do the same stacking as in the observations, and make predictions of the expected ISW signal in the concordance cosmology.

We follow a procedure similar to that of G08 for stacking superstructures, with the key difference being that we scale the filter radius to each void. In G08, a constant filter radius was used because photometric redshift errors prevented accurate estimates of physically meaningful void radii. In contrast, the current sample allows more accurate estimates.

The filtered CMB signal around each void is the temperature averaged over a circular aperture $r < R$ around the void center, minus the temperature averaged over a surrounding annular aperture $R < r < \sqrt{2}R$:

$$\Delta T = \bar{T}_1 - \bar{T}_2 = \frac{\int_0^R T(\boldsymbol{r})d\boldsymbol{r}}{\int_0^R d\boldsymbol{r}} - \frac{\int_R^{\sqrt{2}R} T(\boldsymbol{r})d\boldsymbol{r}}{\int_R^{\sqrt{2}R} d\boldsymbol{r}}, \quad (4)$$

where R is the radius of the filter. We use ΔT for filter temperature and reserve T for the unfiltered temperature throughout the paper. The main purpose of this filter is to suppress large-scale power contamination from the primordial CMB. In reality, void profiles are not compensated top-hats, and this filter is likely not the optimal for ISW detection. However, as long as we perform the same convolution for both the real data and simulations, direct comparisons between them are fair and meaningful. This relatively simple convolution enables us to easily adjust the size of the filter according to the size of each void; the optimal ratio of the filter size R and the ZOBOV void size is determined from simulations.

With this aim, simulated voids of similar radii at the same redshifts are stacked. This is done for both the halo number-density field and the 3D ISWRS signal, i.e., $\dot{\Phi}$ on a 3D grid. Then, the stacked 3D grids of $\dot{\Phi}$ are projected along all three axes of the cubic simulation box. This yields the two-dimensional (2D) stacked ISWRS temperature ΔT map, as shown on Figure 1(A). A cold spot corresponding to the stack of 475 voids is clearly seen, as expected. The outflow of dark matter indicated by the mass-weighted velocity field (shown in arrows in Figure 1(A)) explicitly shows that the stacked void region is expanding. The map is then convolved with compensated top-hat filters of different radii, from which filtered ISWRS temperatures corresponding to the void region are found.

Here we see that quasilinear or nonlinear-scale voids generally have overdense shells around them. Indeed, that is roughly the definition of a ZOBOV void. The ISWRS signals of these nonlinear voids generally have hot rings around them, as shown in the green curve of Figure 1. Therefore, although it has been argued that an uncompensated filter is of equal value in detecting features in the CMB (Zhang & Huterer 2010), at least for detection of an ISW-like void or supercluster imprint, use of a compensated filter is justified and greatly preferred.

4.2. Optimizing the Filter Size

To find the optimal filter radius for a given void effective radius, we explore a wide range of filter radii in our simulations. Figure 1(B) shows the filtered ISWRS temperature versus filter radius R for voids of the average radius $r_{\rm v} \sim 49$ Mpc h^{-1} (red line). We also plot the cumulative ISWRS temperature profile without convolution with the filter in green and the 3D halo density profile in orange. Interestingly, we find that the filtered ISWRS signal peaks at $R \sim 0.6r_{\rm v}$, i.e., at significantly smaller values than the measured void radius, roughly coinciding with the zero-crossing of the ISWRS temperature profile. The optimal filter size appears to be independent of redshift. It is a weak function of the void radius, increasing to approximately 0.7 for $r_{\rm v} > 70$ Mpc h^{-1}. For the SDSS analysis, we implement this nearly universal filter size as a "rescaling factor" before stacking.

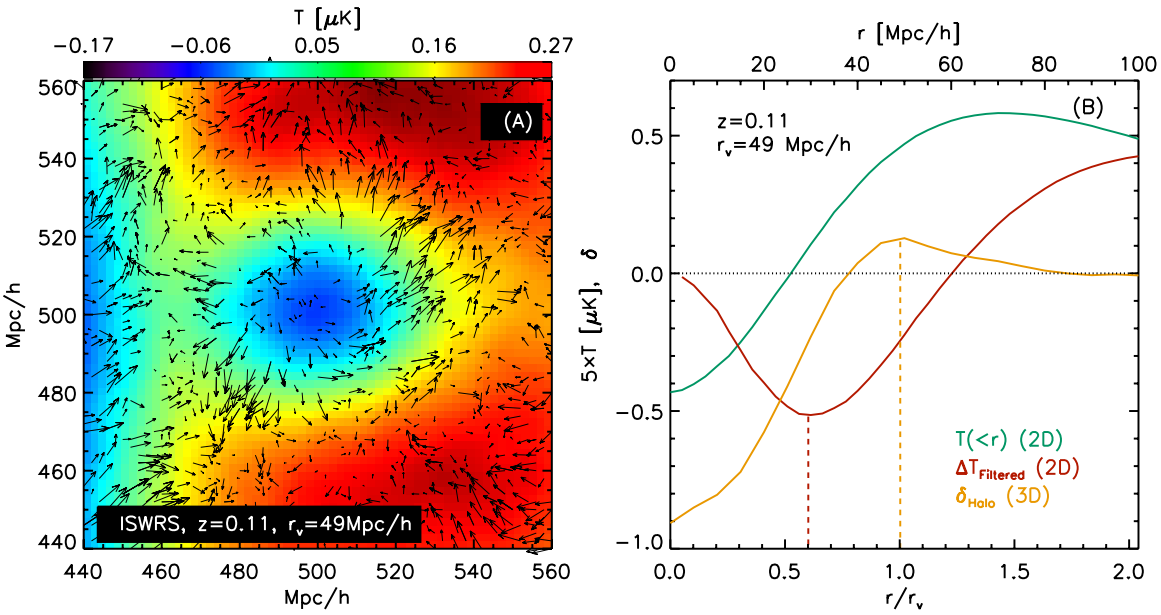

Figure 1. From *N*-body simulations, the stacked ISWRS 2D temperature (panel (A)) and the one-dimensional average cumulative temperature profile (green solid curve in panel (B)) for simulated voids with radius $r_v \approx 49$ Mpc h^{-1}. Arrows are the mass-weighted velocity of the dark matter, indicating the outward expansion of matter from the center of the ISW cold spot. In panel (B), 3D void density profiles traced by halos are shown in orange. The red solid line is obtained from convolving the average 2D projected ISWRS temperature map with compensated top-hat filters of different radii *R*. The red dashed line indicates the filter radius where the ISWRS temperature reaches its minimum (maximum in absolute value). It is about 60% of the effective void radius traced by halo number density, as indicated by the orange dashed line. The zero-crossing of the green curve is very close to the radius where the filtered ISWRS signal peaks. These profiles come from the stacking of 475 voids within the radius of 45–55 Mpc h^{-1}, identified by using halos at $a = 0.9$ from the simulation with the box size of $L = 1000$ Mpc h^{-1}. For the ISWRS maps, Fourier modes with $k < 0.01$ h Mpc^{-1} are removed to reduce the noise. The temperatures on panel (B) are multiplied by a factor of five for better illustration.

(A color version of this figure is available in the online journal.)

Compared with the density field, the potential (and its time derivative) carries an extra factor of $1/k^2$, causing scales much larger than the voids in the catalog to dominate the ISWRS temperature maps. To reduce this large-scale variance, we remove some very large-scale modes ($k < 0.01$ h Mpc^{-1}) when showing the ISWRS temperature map and profiles. Even with the k-mode removal and the stacking of 475 voids, the ISW cold spot still does not seem very circular; there is still substantial noise. Indeed, when analyzing subsamples, we found many fluctuations in the 2D map (Figure 1(A)) and in the uncompensated average temperature as a function of radius (the green line of Figure 1(B)). However, the compensated-filtered temperature in Figure 1(B) remained quite stable; this is another justification for using a compensated filter. It is reassuring that the halo-density profile (yellow line) matches expectation for a void profile.

4.3. Optimizing the Void Catalog

Naively, to avoid a posteriori bias, one may simply take the entire void catalog for stacking the CMB. However, this is risky in that (1) voids found in galaxy catalogs might not correspond to real voids in the density field. If the sampling is sparse, only large voids can be detected. (2) There are voids whose sizes are about the same as the mean galaxy separations for each volume-limited sample, which may be spurious. (3) It is known that some voids, in particular small ones, may live in overdense environments, where the large-scale environment might be contracting. These so-called voids-in-clouds (e.g., Sheth & van de Weygaert 2004; Ceccarelli et al. 2013; Hamaus et al. 2013) could generate ISW hot spots on a larger scale than the detected void, and it is unclear that our compensated filtering would be sufficient to pick out a cold spot.

We note also a previously unappreciated reason why the smallest voids in a halo sample might tend to reside in larger-scale overdensities. Large-scale overdense patches have higher halo number density and thus higher sampling than average. High sampling is exactly what is needed to resolve the smallest voids, so it is not surprising that a sample of only the smallest voids would tend to be in large-scale overdense regions.

Figure 2 shows an ISWRS stack using relatively small voids, $r_v \sim 20$ Mpc h^{-1}. We find from the stacked halo number density profile (panel (B)) that the voids are indeed real underdense regions. However, stacking their CMB imprints yields a large hot spot with the radius of more than 80 Mpc h^{-1}. This suggests that those relatively small voids are likely to live in overdense environments which are contracting. Indeed, the mass-weighted velocity field overplotted in panel (A) indicates convergent flow of dark matter toward the stacked void center. (We notice that the large-scale hot spot is slightly off-centered, most likely due to cosmic variance introduced by large-scale modes.) It is not ideal to blindly take voids defined in the halo density field for the ISWRS stacking procedure. The void-in-cloud problem may reduce the total stacked signal or even reverse the sign of it. It also complicates the interpretation of the stacked ISWRS signal. To tackle this problem, we turn to our simulations.

In simulations, we stack voids in relatively narrow ranges of radii (5 Mpc h^{-1}) at each redshift of our simulations, applying the optimal rescaling filter radius for the compensated filter to obtain the stacked, filtered ISWRS temperature. Results are shown in Figure 3. The ISWRS temperature clearly depends on size and redshift, i.e., larger voids induce a greater ISWRS signal. A void at constant r_v has larger $|\Delta T|$ at larger scale factor, indicating the increasing influence of dark energy. Voids with $r_v < 20$ Mpc h^{-1} have $|\Delta T| < 0.1$ μK at all redshifts. The largest voids found in the SDSS data ($r_v \sim 140$ Mpc h^{-1}) may

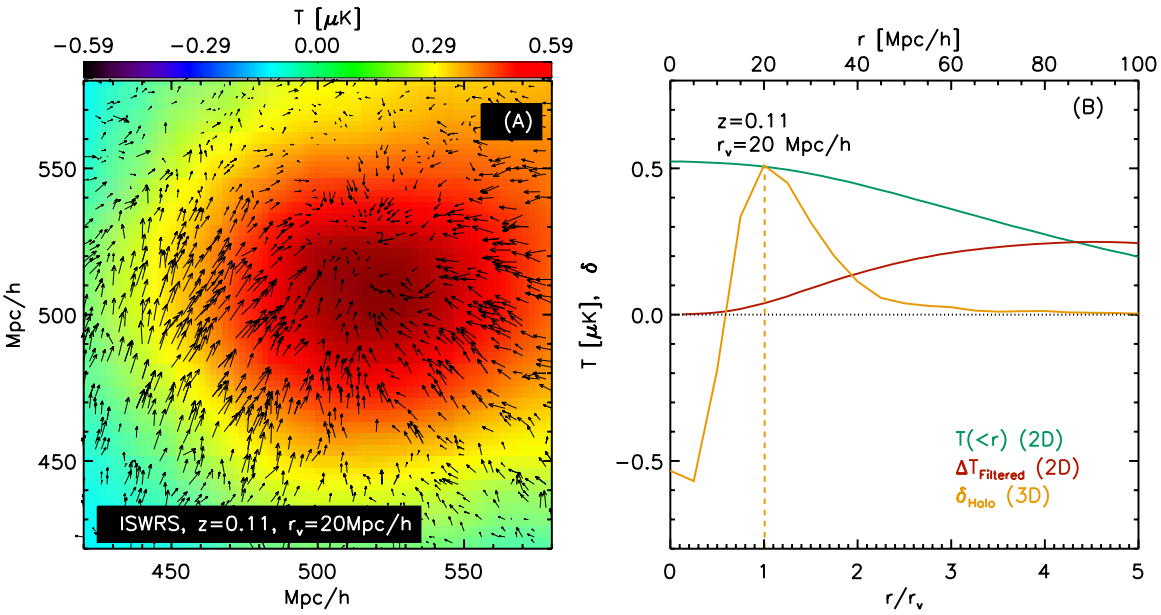

Figure 2. Same as Figure 1 but for stacking simulated voids with radius $r_v \approx 20$ Mpc h^{-1}. There are 626 voids with a radius between 17.5 and 22.5 Mpc h^{-1}; they are identified by using halos at $a = 0.9$ from the $L = 1000$ Mpc h^{-1} simulations. Even though they are true underdensities in the halo number density, as shown in the orange line of panel (B), their stacked ISWRS signal gives a hot spot, as shown in panel (A) and also in green line of panel (B). Arrows in panel (A) are the corresponding mass-weighted velocity of the dark matter, indicating the convergent flow of matter toward the center of the local void region defined by halos.

(A color version of this figure is available in the online journal.)

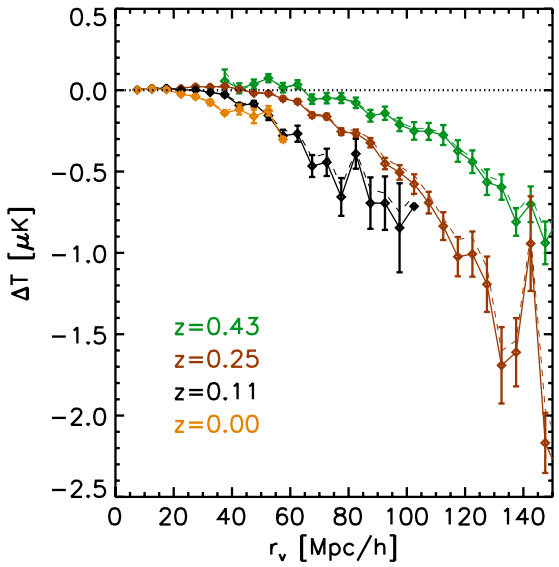

Figure 3. Filtered ISWRS temperature, ΔT, for voids of different radii, r_v, at different redshifts as indicated in the legend. These results are from the simulations but measured as in the observations. Dashed lines indicate the linear ISW signal. We linearly interpolate the zero-crossings of these curves to determine the cuts in the void radius to apply to the SDSS DR7 void catalog.

(A color version of this figure is available in the online journal.)

have $|\Delta T| \sim 1$–2 μK, but they are very rare. The magnitude of the linear ISW signal is typically 10%–20% lower than the full ISWRS signal. Larger differences are found for smaller voids such as $r_v < 20$ Mpc h^{-1}, but the overall amplitudes there are negligibly small.

Notice that each colored curve crosses zero at low void radius and stays close to zero. This is an indication of the effect shown in Figure 2, or it could possibly be a sign of spurious voids. To get rid of them, we draw cuts in the void radius on the basis of the zero-crossings of those simulated curves for each volume-limited sample. They are $r_{\rm cut,default} = [20, 25, 30, 35, 45, 65]$ Mpc h^{-1}, where two of them are from interpolations. Unfortunately, the majority of the voids in DR7 are smaller than those sizes. With these cuts, we throw away two thirds of the 1521 voids, retaining only 477 voids. If the signal corresponds to what we find in simulations, this should ensure that, on average, the stacked ISWRS signal for voids is negative.

These cuts may seem overconservative, but the expected signal-to-noise ratio (S/N) for the ISWRS signal from an individual void is so small that it can be easily swamped by the noise. It is worth making an aggressive cut to reduce the noise if we have good physical reasons. We will investigate this issue further in Section 4.5. In the next subsection, we apply these cuts to the real data and present our main results on these relatively clean void catalogs.

4.4. Stacking with SDSS Data

In individual voids, the expected ISWRS signal we are interested in is overwhelmed by two major sources of noise: (1) the primordial CMB temperature fluctuations and (2) the ISWRS temperature fluctuations that have larger coherent scales than the typical size of our voids. These noise sources, which are essentially cosmic variance, are much greater than the ISWRS signal for which we are looking. It is therefore necessary to try to suppress them to see the potential ISWRS signal. For this purpose, we use two techniques. First, we remove large-scale modes from the CMB, i.e., $\ell \leqslant 10$, knowing that these scales are much larger than the sizes of our voids and the sought ISWRS signal will not be affected by the removal of them. All results we show in the rest of the paper have the $\ell \leqslant 10$ restriction unless specified otherwise. Second, we apply compensated top-hat filters to the CMB, hoping to further reduce the influence of large-scale modes. Of course, stacking a large number of voids can also help to reduce the noise, but we are limited by the size of the current data.

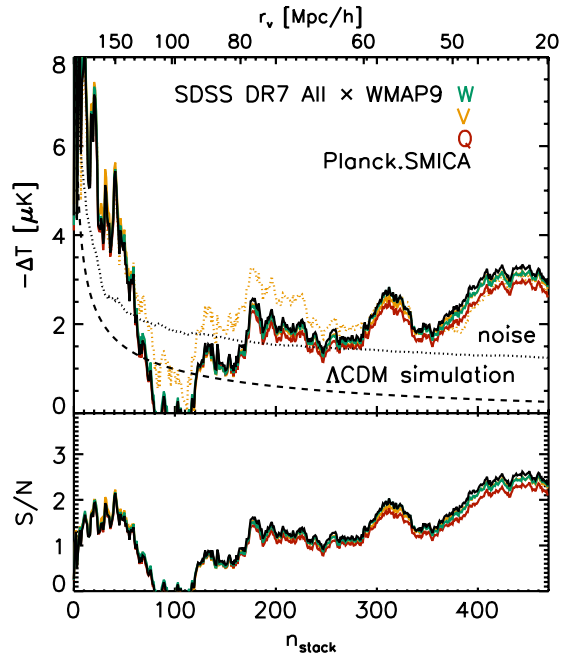

Figure 4. Stacking of the *WMAP*9 *Q* (red), *V* (orange), and *W* (green) bands and the *Planck* SMICA maps using void catalogs from the SDSS DR7 galaxy sample. In the upper panel, solid curves show cumulative stacks of the compensated-filtered CMB temperature. Voids are sorted by size, which increases from the left to the right. The orange dotted curve is similar to the orange solid curve, but each void is weighted by its probability of not being random in a Poisson model, according to Equation (5). See Figure 6 and Section 4.5 for more detail. The black dotted line is the variance calculated from randomizing the sky position of each void 1000 times and repeating the stacking. The dashed line is the stacked linear+nonlinear ISWRS signal in the fiducial concordance cosmology using simulated void catalogs described in Section 4.2. The lower panel shows the cumulative signal-to-noise ratio (S/N) for each stack. After stacking about 200 voids, we get a $\sim 2\sigma$ detection.

(A color version of this figure is available in the online journal.)

We use the *WMAP*9 foreground-reduced *Q*, *V*, and *W* frequency maps (Bennett et al. 2013) for the stack, excluding voids that overlap by >20% with *Wilkinson Microwave Anisotropy Probe* (*WMAP*) masked regions. This reduces the number of voids slightly, from 477 to 470. We then use the void centers for stacking the CMB maps, rescaling the CMB according to the effective radius of each void and applying the compensated filter to it. The filter for each void is scaled to 60% of the radius, the scaling factor found in simulations. The solid lines on the top panel of Figure 4 show the cumulative stacked CMB temperature ΔT versus the number of stacks. The stacked CMB temperature is negative for almost all $n_{\rm stack}$, an indication of the stability of the signal. The stacked temperature varies from -2 μK to -3 μK after stacking $\sim$150 voids. When all the 470 "cleaned" SDSS voids are used for stacking, the resulting filtered temperatures show little frequency dependence; they are -2.6, -2.8, and -2.8 μK in the *Q*, *V*, and *W* bands, respectively. This is consistent with an ISWRS-like signal.

To estimate the statistical significance, we measure the noise in two ways. First, we keep the sizes and relative positions of all voids fixed and randomly rotate them on the CMB map before stacking. The *WMAP* mask is applied in the same way as we do for the original stacking. We estimate the variance of the stacked temperatures from 5000 of such randomizations. The resulting 1σ variation is shown as the dotted curve in Figure 4. Second, we use the best-fit CMB power spectrum (Larson et al. 2011) to generate 5000 mock CMB maps and repeat the same stacking procedure with them. The variances of the random sample are nearly the same as those from the first method at the percent level. This indicates the robustness of noise estimation.

The S/N of the stack is shown in the bottom panel of Figure 4. With a certain amount of random fluctuation, the S/N is in general increasing with the number of voids in the stacks. After stacking $\sim$150 voids, it reaches $\sim 2\sigma$. The stack of all cleaned SDSS voids yields $\sim$2.1, 2.2, and 2.2σ for the *WMAP*9-*Q*, *V*, and *W* bands.

For the stacking, we have also tried using the *Planck* SMICA map (Planck Collaboration et al. 2013a) with the same *WMAP*9 mask, and we find $\Delta T \sim -2.9$ μK, which is about 2.3σ, slightly higher than *WMAP* results, but the differences are negligible. The black solid lines in Figure 4 show that the cumulative stacking signal with *Planck* is also very similar to those from the *WMAP* bands. It is reassuring that switching from *WMAP*9 maps to *Planck* SMICA, with much higher resolution ($N_{\rm side} = 2048$), yields the same results.

Qualitatively, this negative temperature fluctuation corresponding to the stacking of voids is expected from the linear ISW effect in the ΛCDM universe. Therefore, this signal, although it is marginal in significance, suggests that the universe at $0 < z < 0.44$ is accelerating in its expansion. We make a quantitative comparison of the signal with that expected in ΛCDM using our simulations. From the simulated mean filtered ISWRS temperature ΔT for voids of different sizes at different redshifts presented in Figure 3, we sample from the table of $\Delta T(r_{\rm v}, z)$ for the 470 voids with the same sizes and redshifts as in the SDSS data, and we obtain the simulated curve of cumulative stacked ΔT versus the number of voids in the stack for this cosmology shown by the dashed line in Figure 4. The magnitude of the simulated ISWRS signal is substantially smaller than the observed one. If there is no other contamination or systematics, the data suggest a $\sim 2\sigma$ tension with the ΛCDM cosmology.

We caution that our $\sim 2\sigma$ measurement of cold imprints of the voids on the CMB is difficult to explain with the ISW effect in a ΛCDM universe. Suppose that in an optimistic case, the expected ISWRS signal is of the order of 1 μK for voids of $r_{\rm v} \sim 100$ Mpc h^{-1}, as shown in Figure 3, and the CMB temperature fluctuation is of the order of 30 μK. Assuming the noise in the stack goes down as $1/\sqrt{N}$, one will need a stack of 8100 voids to make a 3σ detection. This is beyond the reach of any existing data. As another example, if we have voids with radius $r_{\rm v} \sim 50$ Mpc h^{-1} at $z \sim 0.1$ as shown in Figure 1, given the 1 Gpc h^{-1} simulation box size, the projected 2D ISWRS temperature fluctuations are of the order of 10 μK, while the ISWRS temperature from the void is at the order of 0.1 μK. To reach a 2σ (3σ) detection, even without the primordial CMB fluctuations, the number of voids we would need to stack is $\sim$40,000 (90,000). The fact that we have had a $\sim 2\sigma$ signal (if ISW) with 470 voids is somewhat surprising, although again there is a 5% chance of it being noise.

4.5. Robustness Tests

A $\sim 2\sigma$ signal is by no means significant. There is a 5% chance of it being random noise, in which case it may be sensitive to cuts we impose in the catalog. It is therefore instructive to test how the result varies with our selection criteria. To do this, we vary the void size cut around our fiducial choice over a wide range. Another quantity that could be used to remove unphysical voids is the ratio of the density on the ridge, $\rho_{\rm r}$, to its lowest density $\rho_{\rm min}$. A higher value of $\rho_{\rm r}/\rho_{\rm min}$ means the void is more significant. This is a good quantifier of the probability *P* of a

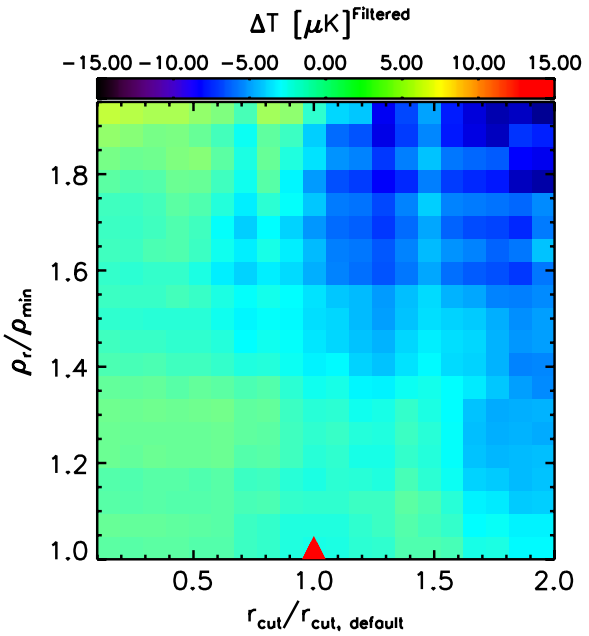

Figure 5. Filtered-stacked temperature as we change the cuts for the void sizes and probability of voids around the fiducial values chosen from simulations. The x-axis is the threshold for void sizes compared with the fiducial cuts; on the right, only the largest voids are kept. The y-axis is a threshold in a measure of the statistical significance of a void. Higher $\rho_r/\rho_{\rm min}$ is more significant. The red triangle indicates the result from the default cuts of $r_{\rm cut}/r_{\rm cut,default} = 1$ and $\rho_r/\rho_{\rm min} = 1$. Its value corresponds to the value of ΔT where the yellow curve ends at the right of Figure 4.

(A color version of this figure is available in the online journal.)

void being real (one minus the probability of it arising in a Poisson process),

$$P = 1-\exp\left[-5.12(\rho_r/\rho_{\rm min}-1) - 0.8(\rho_r/\rho_{\rm min}-1)^{2.8}\right] \quad (5)$$

(Neyrinck 2008). This ratio is also essentially the quantity known as persistence, a common measure of a feature's robustness in computational topology (e.g., Sousbie 2011).

In Figure 5, we show the mean CMB imprints of void samples characterized by different cuts in these two quantities. The result from our fiducial cuts, as used in Figure 4, correspond to the pixel value at ($r_{\rm cut}/r_{\rm cut,default} = 1$, $\rho_r/\rho_{\rm min} = 1$), indicated by the red triangle. Pixels at larger $r_{\rm cut}/r_{\rm cut,default}$ represent results from stacking voids of larger radii, while those with larger $\rho_r/\rho_{\rm min}$ are from stacking voids of greater significance. Note that $r_{\rm cut}/r_{\rm cut,default}$ constitutes an array of separate $r_{\rm cut}$ thresholds in each of the six subsamples, since each has its own mean galaxy separation. This is different from the case of treating voids of all the six subsamples together, sorting them, and thresholding them with one single value of $r_{\rm cut}$, as we do in Figure 4. Overall, the stacked-filtered temperatures remain negative in this wide range of selection criteria. Moreover, there is a tendency for the amplitude to increase toward those pixels at the top right corner, suggesting that the amplitude of the signal does increase with the size and the significance of voids, just like the ISW signal would be expected to behave. This suggests that the selection criteria we derive from our simulations are sensible in selecting physically meaningful voids that give cold CMB imprints in the observations.

We also try weighting voids by the probability that they are not spurious Poisson fluctuations, according to Equation (5). This reduces the parameter space to one dimension, $r_{\rm cut}/r_{\rm cut,default}$ (Figure 6). Overall, as we raise the criteria for $r_{\rm cut}/r_{\rm cut,default}$, the amplitude of the weighted-stacked-filtered temperature is increasing (with exceptions at $r_{\rm cut}/r_{\rm cut,default} \sim 1.5$) (left-hand panel of Figure 6), and the (effective) number of voids that passes the criteria also drops, as expected. As in Figure 5, this increase in signal with minimum void radius is similar to that seen in Figure 5, again suggesting that the putative signal is stable. The right-hand panel of Figure 6 shows the dependence of the S/N on $r_{\rm cut}/r_{\rm cut,default}$. The S/N fluctuates from 0.7 to 2.5 and has a tendency to increase with $r_{\rm cut}/r_{\rm cut,default}$. Our fiducial cut (as indicated by the red triangle) happens to be at a local maximum but not at the global one.

To qualitatively see that our results shown in Figure 4 may be affected by Poissonian confusion, we give one example of the cumulative stacked-filtered temperature weighted by the void probability, shown in the orange dotted curve in Figure 4. The curve shows slightly smaller fluctuations than the orange solid curve when the number of voids used for stacking is relatively small. In particular, a few large voids of lower probability have been down-weighted (at $n_{\rm stack} \sim 100$) such that the stacked temperature is prevented from going positive, hence the amplitude of the stacked-filtered temperature is increased. This suggests that the void-probability weighting scheme is helpful in reducing Poisson fluctuations by down-weighting voids of low probability. However, as $n_{\rm stack}$ increases, or r_v drops, weighting or not weighting makes little difference. The void-probability weighting scheme seems to be inefficient for helping to increase the signal. This may suggest that for relatively small voids, whether their filtered ISW temperatures are negative or positive depends more strongly on their environments, i.e., void-in-cloud or void-in-void. The stacked signal depends weakly on void probabilities.

We emphasize that results shown in Figures 5 and 6 are merely a robustness test of our analysis. Seeing that there might be a larger signal for larger voids and more significant voids, we do not, however, change our the selection criteria and claim a higher-significance detection; this would constitute a posteriori bias.

Finally, we also try varying the rescaling factor for the size of the filter radius. Results are shown in Figure 7. Intriguingly, the same scaling factor of 0.6 that gives the largest amplitudes of the filtered ISWRS temperature in the simulations also gives nearly the largest signal in the data (0.7 in the data). This consistency with simulations regarding the optimal filter size is encouraging. It also seems to suggest that the measured signal may have profiles similar to the simulated ISWRS signal (when comparing Figure 7 with the red curve of Figure 1(B)). For these results, only results from the *WMAP*9-*V* band are shown for better illustration. The same tests with other *WMAP* bands and *Planck* SMICA give similar results.

5. DISCUSSION AND CONCLUSIONS

We have found that stacking CMB temperatures around the positions of voids from the SDSS DR7 spectroscopic galaxy catalog yields a temperature decrement between 2.6 and 2.9 μK, at about 2σ significance. When interpreted as the ISW and the RS effect, it is at odds with simulations of a ΛCDM universe at $\sim 2\sigma$. We want to emphasize that our analysis is based strongly on simulations, which are very important in calibrating the raw data and methodology. In particular,

1. We have found a scaling factor for the compensated top-hat filter radius that optimizes the ISWRS detection. This factor is 0.6 times the effective void radius. In Ilić et al. (2013) and

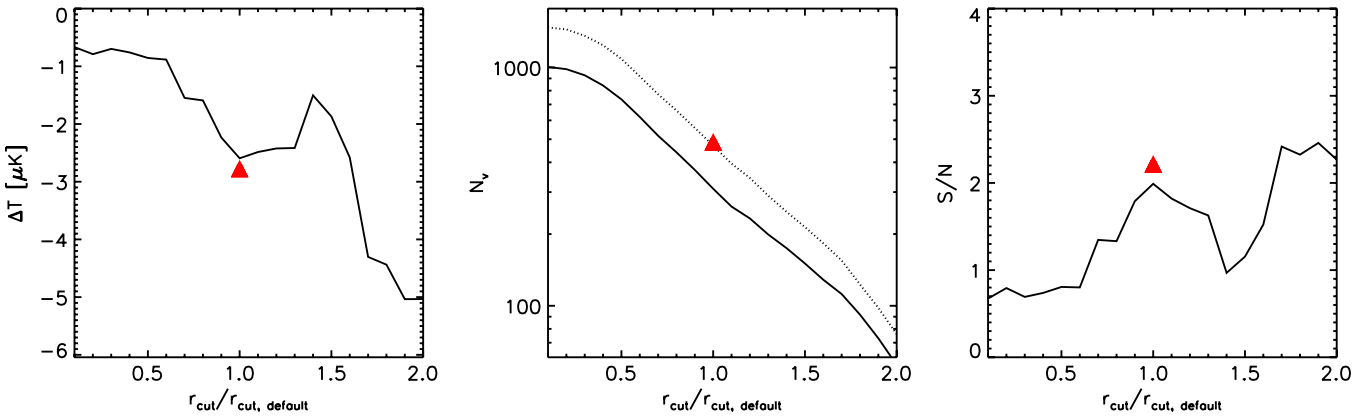

Figure 6. Left: filtered temperature vs. minimal void radius; each void is weighted by its probability of not being random in a Poisson model. Middle: number of voids remaining in the sample as minimal void radius increases (solid), and the effective number of voids (void-probability weighted; dotted). Right: estimated signal-to-noise ratio. The red triangle in each plot indicates the default cuts of $r_{\rm cut}/r_{\rm cut,default} = 1$ and $\rho_{\rm r}/\rho_{\rm min} = 1$. Its value on the left-hand panel corresponds to the value of ΔT where the yellow curve ends at the right of Figure 4. Its value in the middle figure is the number of voids left after applying the default cuts. Its value on the right-hand panel corresponds to the final S/N in Figure 4.

(A color version of this figure is available in the online journal.)

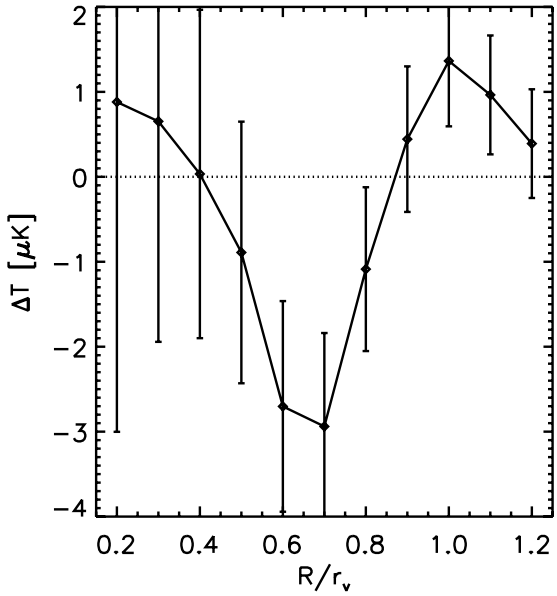

Figure 7. Observed, stacked void signal viewed through compensated top-hat filters of different radii R, relative to the void radius r_v, for comparison with the red curve in Figure 1(B).

Planck Collaboration et al. (2013b), where similar analyses have been done independently with a similar void catalog, there is a strong indication that such a factor is needed to have the best S/N detection in the data. This suggests that there is indeed some (low-level) indication of an ISWRS signal in the data.

2. We emphasize two issues for void catalogs found using tracers of the density field: Poisson noise and environmental effects. There can be spurious voids from Poisson sampling. Also, voids live in different environments with different dynamical properties, and hence the ISWRS signal produced varies. A small void in an overdense region that is contracting will correspond to an ISW hot spot greater than the size of the void. These issues are crucial to consider when pruning a void catalog for ISWRS analysis.
3. We use our simulations to clean up the "raw" void catalog, which is potentially noisy and unlikely to be optimal for ISW analysis. While our fiducial cuts on the void catalog might be conservative, the results seem to be robust when varying our thresholds around the fiducial ones. Interestingly, the signal increases if only the largest and most statistically significant voids are used, just as expected if the signal is the ISW effect.

Stacked CMB temperature maps using voids should suffer little contamination from other astrophysical processes, in that voids are relatively empty. The frequency independence of the result shown in the previous section suggests that it is unlikely to come from contamination by radio sources or the thermal SZ effect (Sunyaev & Zeldovich 1972). It is also unlikely to be contaminated by the kSZ effect, which arises from the line-of-sight bulk motion of free electrons relative to the CMB. For the kSZ effect to induce the observed temperature decrement in voids, a void would have to have a high column density of free electrons, which is unlikely.

Our measured average imprint somewhat bolsters the results of Granett et al. (2008, G08) and vice-versa. The signals both go the same way and have a larger amplitude than expected in a ΛCDM universe. Our fiducial measured imprint is ∼10 times greater than expected in ΛCDM, although again we strongly caution that its statistical significance is only $\sim 2\sigma$. The G08 statistical significance was 4.4σ including both voids and clusters and 3.7σ including only the voids. Note that the present result is not entirely independent of G08, since they both use the CMB in the SDSS footprint, and there is a tiny overlap in redshift; this sample spans $z = 0$–0.44, while the G08 sample spans $z = 0.4$–0.75.

In principle, the tension between the detection of the ISWRS signal with the ΛCDM model could be resolved by invoking non-Gaussianity. However the value of $f_{\rm NL}$ needed may be at the order ∼1000 (Hernandez-Monteagudo & Smith 2013), which is inconsistent with constraints from the CMB (e.g., Komatsu et al. 2011; Planck Collaboration et al. 2013c). Alternatively, voids in some models of modified gravity may grow larger and faster than in the ΛCDM universe, giving a larger ISWRS signal Clampitt et al. (2013). Whether or not such models can tolerate the high amplitude of the ISWRS signal while not violating other observational cosmological constraints remains an open question. Further investigation of this issue with surveys of larger volume and sky coverage is also needed to firmly confirm

and resolve this tension. See an ISW study in the $f(R)$ modified gravity model in Cai et al. (2014).

Throughout our paper, we have used our own algorithm to find voids in the SDSS volume-limited samples. Sutter et al. (2012) applied a similar pipeline to the same SDSS DR7 data sets and constructed a public void catalog. We notice that while these two catalogs are similar in many aspects, there are subtle differences that may affect the ISW analysis. However, it is beyond the scope of our paper to understand how the two catalogs differ. Nevertheless, we make our version of the void catalog public. The Sutter et al. (2012) catalog has been used for the analysis of Ilić et al. (2013) and Planck Collaboration et al. (2013b). It is perhaps more valuable to have an relatively independent analysis. Also, Ilić et al. (2013) and Planck Collaboration et al. (2013b) both have found some indications of a "2σ" signal by using all of the Sutter et al. (2012) catalog at a filter scale radius of $\sim$0.6. In light of our calibration with simulations, this is exactly where the optimal signal is to be expected. Interestingly, with different catalogs and independent analysis pipelines, there are still suggestions of an ISWRS signal.

Finally, we note that although we have made significant progress toward optimal ISW analysis with voids through calibration with simulations, there is still room for improvement. Compensated filtering is essential, but the top-hat shape is likely not optimal; for example, the signal through a Mexican hat filter is more stable to changes in filter radius. Also, the optimal technique would likely involve an inverse-noise weighting for each void, which would involve ISWRS signals measured in simulations, as well as the expected "noise" from the primordial CMB. In this paper, we have kept our methodology close to that of previous works for comparison, but optimizing the method for ISWRS detection remains an interesting subject for future work.

We thank P. M. Sutter for his helpful discussions and comments on an earlier version of the manuscript and and S. Nadathur for useful comments on our later version. We thank the referee for a helpful report. We thank Baojiu Li for providing the *N*-body simulations. M.N. is grateful for support from a New Frontiers grant from the Sir John Templeton Foundation. Y.C. is supported by the Durham Junior Research Fellowship. I.S. acknowledges NASA grants NNX12AF83G and NNX10AD53G for support. Y.C., S.C., and C.F. acknowledge the support of the Science and Technology Facilities Council (grant number ST/F001166/1). Part of the calculations for this paper were performed on the ICC Cosmology Machine, which is part of the DiRAC Facility jointly funded by STFC, the Large Facilities Capital Fund of BIS, and Durham University. Some of the results in this paper are derived using the HEALPix package (Górski et al. 2005).

Funding for the SDSS and SDSS-II has been provided by the Alfred P. Sloan Foundation, the Participating Institutions, the National Science Foundation, the U.S. Department of Energy, the National Aeronautics and Space Administration, the Japanese Monbukagakusho, the Max Planck Society, and the Higher Education Funding Council for England. The SDSS Web site is http://www.sdss.org/.

The SDSS is managed by the Astrophysical Research Consortium for the Participating Institutions. The Participating Institutions are the American Museum of Natural History, Astrophysical Institute Potsdam, University of Basel, University of Cambridge, Case Western Reserve University, University of Chicago, Drexel University, Fermilab, the Institute for Advanced Study, the Japan Participation Group, Johns Hopkins University, the Joint Institute for Nuclear Astrophysics, the Kavli Institute for Particle Astrophysics and Cosmology, the Korean Scientist Group, the Chinese Academy of Sciences (LAMOST), Los Alamos National Laboratory, the Max-Planck-Institute for Astronomy (MPIA), the Max-Planck-Institute for Astrophysics (MPA), New Mexico State University, Ohio State University, University of Pittsburgh, University of Portsmouth, Princeton University, the United States Naval Observatory, and the University of Washington.

REFERENCES

Bennett, C. L., Larson, D., Weiland, J. L., et al. 2013, ApJS, 208, 20
Bielby, R., Shanks, T., Sawangwit, U., et al. 2010, MNRAS, 403, 1261
Cai, Y.-C., Cole, S., Jenkins, A., & Frenk, C. 2009, MNRAS, 396, 772
Cai, Y.-C., Cole, S., Jenkins, A., & Frenk, C. S. 2010, MNRAS, 407, 201
Cai, Y.-C., Li, B., Cole, S., Frenk, C. S., & Neyrinck, M. 2014, MNRAS, 439, 2978
Ceccarelli, L., Paz, D., Lares, M., Padilla, N., & Lambas, D. G. 2013, MNRAS, 434, 1435
Clampitt, J., Cai, Y.-C., & Li, B. 2013, MNRAS, 431, 749
Crittenden, R. G., & Turok, N. 1996, PhRvL, 76, 575
Davis, M., Efstathiou, G., Frenk, C. S., & White, S. D. M. 1985, ApJ, 292, 371
Eisenstein, D. J., Annis, J., Gunn, J. E., et al. 2001, AJ, 122, 2267
Flender, S., Hotchkiss, S., & Nadathur, S. 2013, JCAP, 02, 013
Giannantonio, T., Crittenden, R., Nichol, R., & Ross, A. J. 2012, MNRAS, 426, 2581
Giannantonio, T., Scranton, R., Crittenden, R. G., et al. 2008, PhRvD, 77, 123520
Górski, K. M., Hivon, E., Banday, A. J., et al. 2005, ApJ, 622, 759
Granett, B. R., Neyrinck, M. C., & Szapudi, I. 2008, ApJL, 683, L99
Hamaus, N., Wandelt, B. D., Sutter, P. M., Lavaux, G., & Warren, M. S. 2013, arXiv:1307.2571
Hernández-Monteagudo, C. 2010, A&A, 520, A101
Hernandez-Monteagudo, C., & Smith, R. E. 2013, MNRAS, 435, 1094
Ho, S., Hirata, C., Padmanabhan, N., Seljak, U., & Bahcall, N. 2008, PhRvD, 78, 043519
Ilić, S., Langer, M., & Douspis, M. 2013, A&A, 556, A51
Komatsu, E., Smith, K. M., Dunkley, J., et al. 2011, ApJS, 192, 18
Larson, D., Dunkley, J., Hinshaw, G., et al. 2011, ApJS, 192, 16
Li, B., Hellwing, W. A., Koyama, K., et al. 2013, MNRAS, 428, 743
López-Corredoira, M., Sylos Labini, F., & Betancort-Rijo, J. 2010, A&A, 513, A3
Nadathur, S., & Hotchkiss, S. 2013, arXiv:1310.2791
Nadathur, S., Hotchkiss, S., & Sarkar, S. 2012, JCAP, 06, 042
Neyrinck, M. C. 2008, MNRAS, 386, 2101
Neyrinck, M. C., Gnedin, N. Y., & Hamilton, A. J. S. 2005, MNRAS, 356, 1222
Pápai, P., & Szapudi, I. 2010, ApJ, 725, 2078
Pápai, P., Szapudi, I., & Granett, B. R. 2011, ApJ, 732, 27
Planck Collaboration, Ade, P. A. R., Aghanim, N., et al. 2013a, arXiv:1303.5072
Planck Collaboration, Ade, P. A. R., Aghanim, N., et al. 2013b, arXiv:1303.5079
Planck Collaboration, Ade, P. A. R., Aghanim, N., et al. 2013c, arXiv:1303.5084
Platen, E., van de Weygaert, R., & Jones, B. J. T. 2007, MNRAS, 380, 551
Rassat, A., Land, K., Lahav, O., & Abdalla, F. B. 2007, MNRAS, 377, 1085
Rees, M. J., & Sciama, D. W. 1968, Natur, 217, 511
Sachs, R. K., & Wolfe, A. M. 1967, ApJ, 147, 73
Sawangwit, U., Shanks, T., Cannon, R. D., et al. 2010, MNRAS, 402, 2228
Schaap, W. E., & van de Weygaert, R. 2000, A&A, 363, L29
Seljak, U. 1996, ApJ, 460, 549
Sheth, R. K., & van de Weygaert, R. 2004, MNRAS, 350, 517
Smith, R. E., Hernández-Monteagudo, C., & Seljak, U. 2009, PhRvD, 80, 063528
Sousbie, T. 2011, MNRAS, 414, 350
Strauss, M. A., Weinberg, D. H., Lupton, R. H., et al. 2002, AJ, 124, 1810
Sunyaev, R. A., & Zeldovich, Y. B. 1972, CoASP, 4, 173
Sutter, P. M., Lavaux, G., Wandelt, B. D., & Weinberg, D. H. 2012, ApJ, 761, 44
Sutter, P. M., Lavaux, G., Wandelt, B. D., & Weinberg, D. H. 2013, arXiv:1310.5067
Watson, W. A., Diego, J. M., Gottlöber, S., et al. 2014, MNRAS, 438, 412
Zhang, R., & Huterer, D. 2010, APh, 33, 69